Nuclear Inst. and Methods in Physics Research, A 927 (2019) 187–193

Contents lists available at ScienceDirect

Nuclear Inst. and Methods in Physics Research, A

journal homepage: www.elsevier.com/locate/nima

Comparison of small collection electrode CMOS pixel sensors with partial and full lateral depletion of the high-resistivity epitaxial layer

Dominik Dannheim [a], Adrian Fiergolski [a], Jacobus van Hoorne [a], Daniel Hynds [a,b], Wolfgang Klempt [a], Thanushan Kugathasan [a], Magdalena Munker [a,*], Andreas Nürnberg [a,c], Krzysztof Sielewicz [a], Walter Snoeys [a], Simon Spannagel [a]

[a] CERN, Geneva, Switzerland
[b] NIKHEF, Amsterdam, Netherlands
[c] KIT, Karlsruhe, Germany

ARTICLE INFO

Keywords:
CMOS sensors with a small collection electrode
Monolithic detector prototype
Analogue performance

ABSTRACT

Large area silicon pixel trackers are currently under development for the High Luminosity upgrade of the LHC detectors. They are also foreseen for the detectors proposed for the future high energy Compact Linear Collider CLIC. For the CLIC tracker a single hit resolution of 7 μm, a timing resolution of a few nanoseconds and a material budget of 1–2 % of radiation length per detection layer are required. Integrated CMOS technologies are promising candidates to reduce the cost, facilitate the production and to achieve a low material budget. CMOS sensors with a small size of the collection electrode benefit from a small sensor capacitance, resulting in a large signal to noise ratio and a low power consumption.

The Investigator is a test-chip developed for the ALICE Inner Tracking System upgrade, implemented in a 180 nm CMOS process with a small collection electrode on a high resistivity epitaxial layer. The Investigator has been produced in different process variants: the standard process and a modified process, where an additional N-layer has been inserted to obtain full lateral depletion. This paper presents a comparison of test-beam results for both process variants, focuses on spatial and timing resolution as well as efficiency measurements.

1. Introduction

The *Compact Linear Collider, CLIC,* is a future option for a linear electron-positron collider in the post-LHC era at CERN [1–4]. CLIC is intended to reach a centre-of-mass energy of up to 3 TeV. To achieve high precision measurements, stringent requirements are imposed on the CLIC detector [5]. A single point resolution of 7 μm and a material budget of $1-2\,\%\,X_0$ per layer are needed for the tracker. Furthermore, a hit time resolution of a few nanoseconds is required, to suppress out-of-time background from beam–beam interactions [6]. To address these requirements, a large area silicon tracker with a surface of approximately $140\,m^2$ is proposed for the CLIC detector. Different technologies are currently under investigation in a broad silicon detector R&D programme. In particular monolithic technologies are attractive candidates for the tracker in view of large surface and low material budget.

The ALPIDE chip, a fully monolithic pixel-chip, has been developed for the ALICE *Inner Tracking System (ITS)* upgrade [7] in a 180 nm CMOS process with a small collection electrode. The Investigator is an analogue test-chip produced using the same underlying process as for the ALPIDE chip. The Investigator pixel layout has been designed to minimise the sensor capacitance to a few fF [8]. In this way, a low analogue power consumption, a low noise and a large signal to noise ratio can be achieved. The original process used for the ALPIDE chip has been modified to achieve full lateral depletion of the sensor volume [9]. Both process variants have been studied and a comparison of the results is presented in this paper.

To study the Investigator performance, various test-beam campaigns have been performed at the CERN SPS, using the CLICdp Timepix3 telescope [10]. The chip calibration as well as its noise characteristics are described in detail elsewhere [11], where also a more detailed description of the test-beam setup and reconstruction is presented. This paper focuses on the comparison of test-beam results for the standard and modified process.

2. Investigator chip

The Investigator chip consists of several sections with different pixel layouts, so called mini-matrices. Several geometrical and electronics parameters have been changed for the various pixel layouts, aiming

* Corresponding author.
E-mail address: magdalena.munker@cern.ch (M. Munker).

https://doi.org/10.1016/j.nima.2019.02.049
Received 12 November 2018; Received in revised form 17 February 2019; Accepted 17 February 2019
Available online 21 February 2019

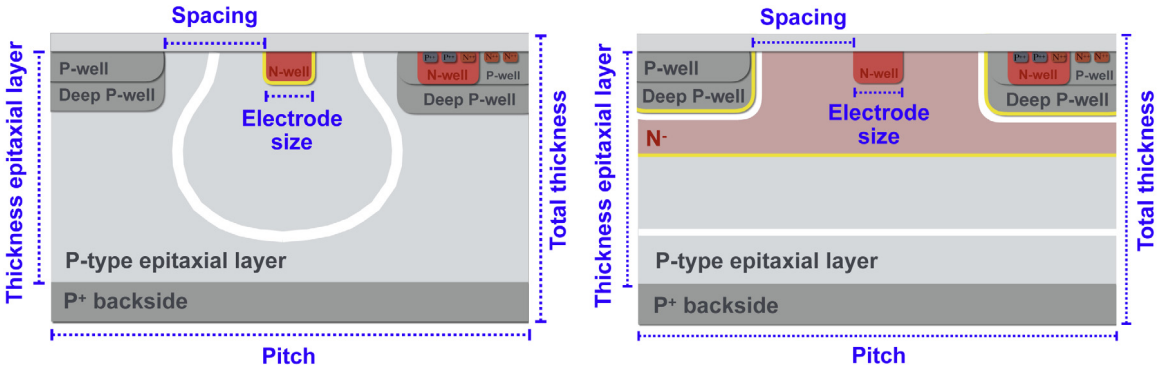

Fig. 1. Schematics (not to scale) of the small collection electrode 180 nm CMOS process used for the fabrication of the Investigator chip in the *standard process (left)* and the *modified process (right)*. The schematic (colour online) represents one unit cell of the periodic pixel matrix. The yellow lines mark the relevant pn junctions. The white lines illustrate the edges of the depleted regions, showing the partial depletion of the standard process and the full lateral depletion of the modified process.

at an optimisation of the efficiency as well as spatial and timing resolution. Each mini-matrix consists of 10×10 pixels, with the 8×8 innermost pixels being read out.

Schematics of the studied small collection electrode 180 nm CMOS processes are presented in Fig. 1. Geometrical parameters of the pixel design are marked. A small sized N-type collection electrode, separated from a P-well containing the CMOS circuitry, is implemented on a high resistivity (1 –8 kΩcm) P-type epitaxial layer. For the *standard process* (left sketch in Fig. 1) a small junction is created around the collection electrode. For the *modified process* (right sketch in Fig. 1) an N-layer is inserted, such that a deep planar junction is created that extends over the full size of the pixel.

A bias voltage is applied to terminals in the P-wells and connected via non-depleted regions at the matrix edges to the backside of the chip. When applying a negative bias voltage, a depleted region starts to extend from the junctions. To avoid breakdown in the NMOS transistor, we limit the absolute bias voltage to 6 V [8]. Due to the small junction and the limited bias voltage the depletion in the standard process is restricted to regions around the collection electrode, while a full lateral depletion can be achieved for the modified process [9].

Each pixel contains a source follower which is located inside the P-wells and converts the charge Q on the diode capacitance C to a voltage $U = Q/C$, as shown in Fig. 2. As a consequence, a particle traversing the sensor manifests itself in a drop of the measured voltage below the pedestal. This voltage drop is relatively large due to the small size of the collection electrode and the resulting small capacitance of the N-well collection diode. Hence, less power is needed to amplify the signal, resulting in a relatively low power consumption. The output of the source follower of each pixel is connected to a dedicated output buffer at the periphery with a rise time of 10 ns. Due to a limited number of output buffers in the periphery of the Investigator, only one mini-matrix can be read out at a time. The studies presented in this paper have been performed for a mini-matrix with a pitch size of 28 µm.

3. INVROS readout system

The Investigator is an analogue test-chip, without any digital logic. Therefore, a dedicated readout system, the *INVROS (INvestigator Read-Out System)*, has been designed to record the full analogue data for each pixel [12]. The INVROS uses one *Analogue to Digital Converter (ADC)* channel per readout pixel, sampling the pixel front end output with a frequency of 65 MHz and 14-bit resolution (AD9249 [13]). If a voltage drop below an adjustable *triggering threshold* value has been observed by the readout system in at least one pixel, the full frame of the amplitudes of the 8×8 read out pixels gets recorded by the INVROS.

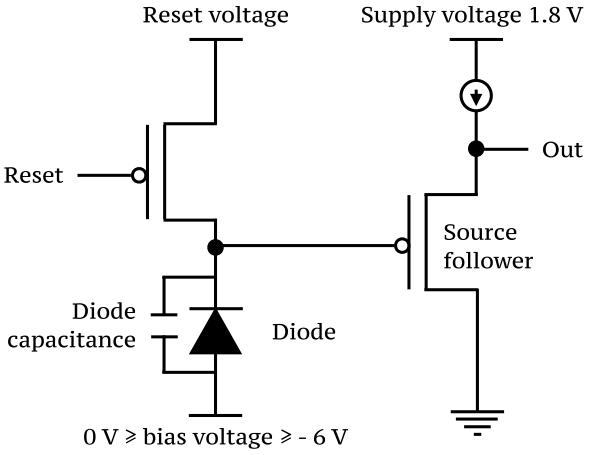

Fig. 2. Simplified single pixel schematic.

4. Test-beam telescope setup

Test-beam measurements have been performed in the H6 beam line of the CERN SPS using a beam of positively charged hadrons with a momentum of 120 GeV. The CLICdp Timepix3-telescoped [10] has been used for particle tracking. With this telescope, a track impact point resolution on the *Device Under Test (DUT)* of ∼2 µm and a track timing resolution on the DUT of ∼1 ns have been achieved.

5. Reconstruction of test-beam data

An offline correction has been applied to filter out common mode noise contributions from the Investigator data [11]. Then, a search for a particle hit is performed for each pixel by comparing the difference in amplitude of each readout sample to the third successive readout sample, as illustrated in Fig. 3.

The signal is defined as the difference of the mean amplitude before and after a particle hit and the noise is defined for each pixel in each event as the *Root Mean Square (RMS)* of the fluctuations of the measured amplitude around the pedestal. An *analysis threshold* has been applied with respect to the noise for each pixel. This analysis threshold can be significantly lower than the triggering threshold during data taking due to the offline correction of the common mode noise. For pixels with a signal higher than the analysis threshold, a constant function followed by an exponential decay starting at the time of the particle hit t_{hit}

$$f(t) = \begin{cases} \text{constant}, & if\ t \le t_{hit} \\ \text{constant} + \text{signal} \cdot (e^{-(t - t_{hit})/t_{rise}} - 1), & if\ t > t_{hit}. \end{cases} \quad (1)$$

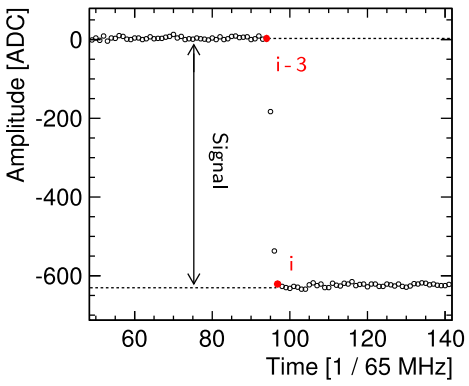

Fig. 3. Procedure to find a first estimate of the hit time.

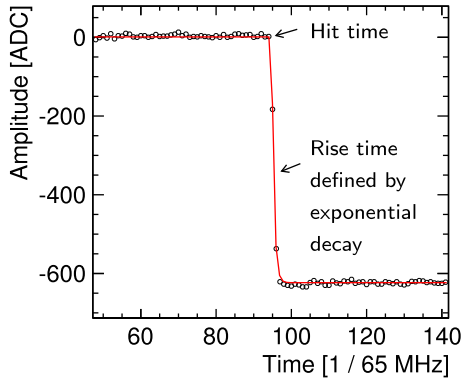

Fig. 4. Fit to single pixel waveform and definition of timing observables.

is fitted to the sampled single pixel waveforms to obtain the timing observables, as depicted in Fig. 4.

Clustering is performed, combining all adjacent pixels exceeding the analysis threshold into a *cluster*. The cluster position is reconstructed using charge interpolation and η-correction [14], to correct for non-linear charge sharing effects. The time of the reconstructed hits is defined as the hit time of the earliest pixel. The time of the track is calculated as the mean time of all hits on the telescope planes associated with the track.

A reconstructed Investigator hit is matched to a reconstructed telescope track, if their spatial separation is smaller than 100 µm. Moreover, the Investigator hit and telescope track need to be within the 10 µs time window of one event, to be matched together. Tracks passing through the outer half of the outermost active pixels of the matrix are discarded. The remaining region on the Investigator chip is referred to

Table 1
Geometrical parameters of the studied Investigator chip and mini-matrix.

Parameter	Value [µm]
Pitch	28
Spacing	3
Collection electrode size	2
Thickness epitaxial layer	25
Overall thickness	100

Table 2
Threshold values, recorded statistics and measured noise values for both process variants [11].

Process	Analysis threshold [e⁻]	Triggering threshold [e⁻]	#roi-tracks	Noise [e⁻]
Standard	40	126	25,660	8
Modified	51	179	24,260	10

in the following as *region of interest (roi)* and tracks passing through that region are referred to as *roi-tracks*.

6. Test-beam results

Results of the standard and modified process are presented for the geometrical parameters specified in Table 1.

Unless mentioned otherwise, the threshold values listed in Table 2 have been applied. All data has been recorded at a bias voltage of −6 V. The measured noise values at this bias voltage after the application of an offline common mode noise filter are also listed in Table 2.

6.1. Charge sharing

The amount of charge shared between neighbouring pixels (*charge sharing*) is affected by the position where the particle passes through the pixel cell. This can be attributed to geometrical effects and variations of the electric field and depleted regions over the pixel cell. Since the geometrical parameters for the study of the standard and modified process are the same, the impact of the different electric field distributions in the sensor for the different processes can be assessed by investigating the dependence of the number of pixels in a cluster (*cluster size*) on the position of the track within the pixel cell. This in-pixel cluster size distribution is shown for the standard and modified process in Fig. 5. Significantly more charge sharing can be observed for the standard compared with the modified process. This is most evident at the pixel edges and corners, where the standard process is not fully depleted, consistent with the illustration of the depleted region in Fig. 1. A contribution of cluster sizes larger than four can be observed in the pixel edges and corners of the standard process, that can be explained by large spread of the charge via diffusion [11].

As visible in Fig. 6, the charge sharing from diffusion in the standard process introduces a stronger correlation of the X cluster size on the

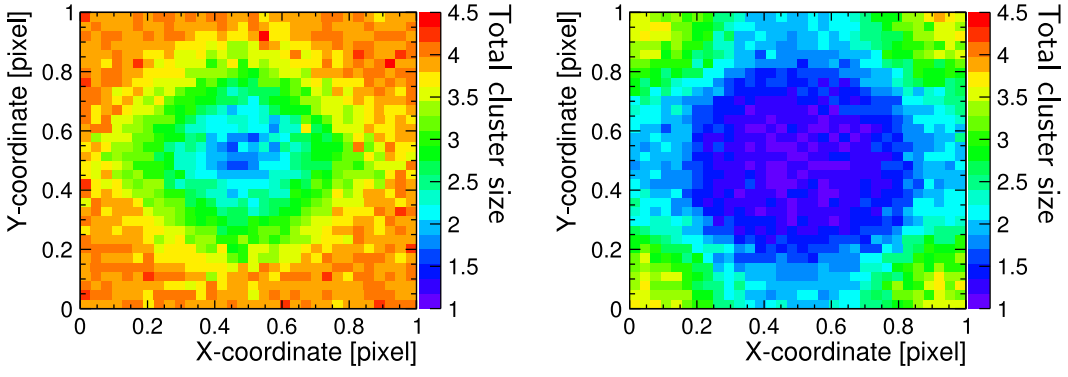

Fig. 5. Total cluster size (colour online) within the pixel cell for the *standard process (left)* and for the *modified process (right)*.

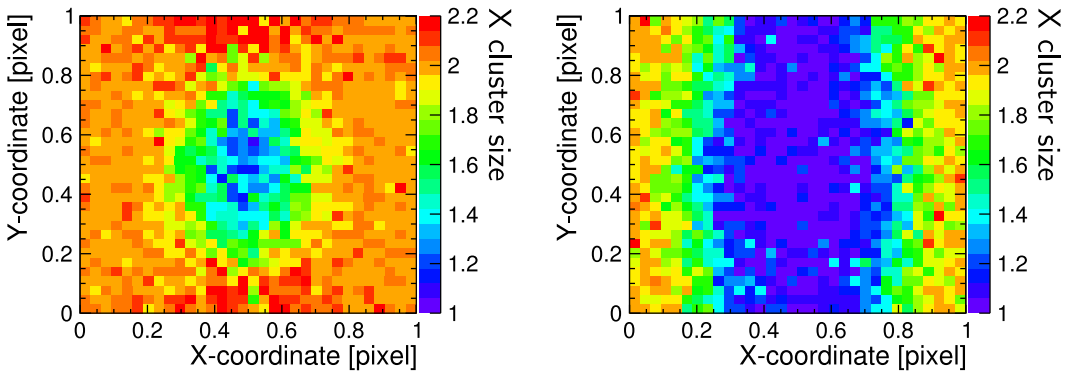

Fig. 6. In-pixel representation of the cluster size in X (colour online) for the *standard process (left)* and the *modified process (right)*.

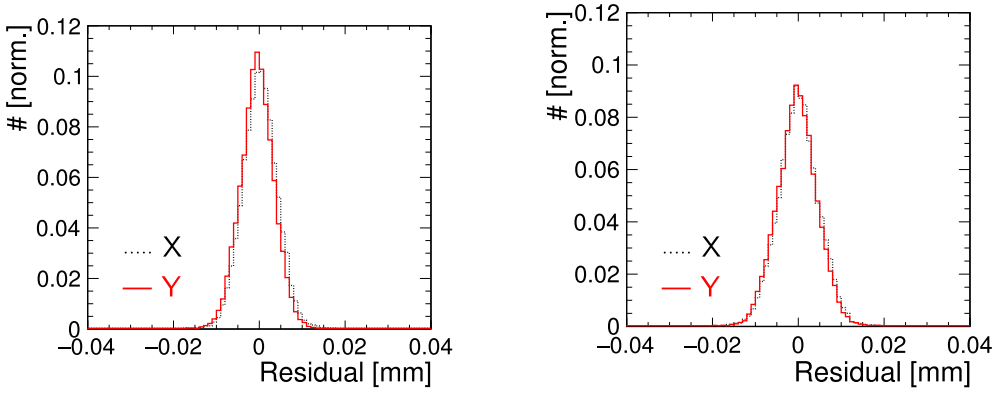

Fig. 7. Spatial residual distributions in X and Y dimension of the pixel matrix for the *standard process (left)* and for the *modified process (right)*.

Y-coordinate of the track intercept (and vice versa). As discussed in Section 6.2, this correlation is not taken into account in the reconstruction of the hit position and might thus degrade the spatial resolution.

6.2. Spatial resolution

Due to the increased charge sharing for the standard process more information is available that can be used for the position reconstruction. The spatial residual distribution is calculated as the difference between the track intercept position on the Investigator and the reconstructed cluster position and is presented in Fig. 7 for the standard and modified process.

A broader distribution has been measured for the modified process, consistent with the reduced charge sharing. Note that the thresholds are not exactly the same in units of electrons, since a fixed multiplicity of five times the noise has been selected for the analysis. The noise is slightly higher for the modified process due to a slightly higher pixel input capacitance. A relative difference of ∼20 % of the input pixel capacitance between the two process variants has been measured using the spectrum extracted from ^{55}Fe measurements [11].

Calculating the central *RMS* of the residual distributions on a range that covers 99.7 % of the statistics ($RMS_{99.7}$), the resolution is determined as

$$\text{Resolution} = \sqrt{RMS_{99.7}^2 - \sigma_{tele}^2} \tag{2}$$

using a telescope resolution of σ_{tele}=1.8 µm [10]. As visible in Fig. 7, the residual distributions have a Gaussian shape at low threshold values. However, at high threshold values the contributions from different cluster sizes lead to a non-Gaussian double peak structure in the residual distributions [11]. For this reason the $RMS_{99.7}$ has been used for the calculation of the resolution instead of the width of a Gaussian fit to the residual distributions. The residual distribution has been restricted to a range containing 99.7 % of the statistics to not be sensitive to outliers.

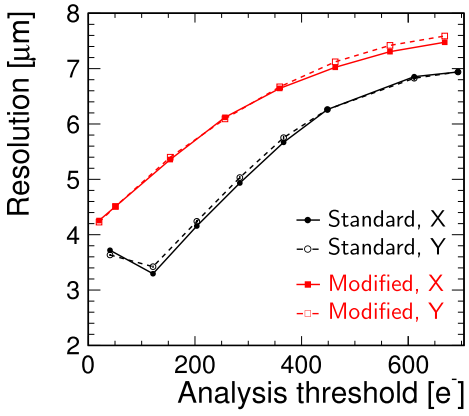

Fig. 8. Resolution in X and Y direction for different analysis thresholds.

The resolution for different analysis threshold values is presented in Fig. 8. The stated statistical uncertainties have been calculated by fluctuating the statistics of each bin of the residual distribution according to a Poisson distribution.

Especially at low threshold values the spatial resolution for the modified process is degraded with respect to the standard process. At very low threshold values the resolution of the standard process degrades again, which might be either attributed to noise or to the observed correlation of the X/Y cluster size with the other coordinate of the track intercept position inside the pixel cell. This is not taken into account when reconstruction is performed separately in X and Y. An optimal spatial resolution of ∼3 µm is reached for the standard process, significantly better than the ∼4 µm in the modified process.

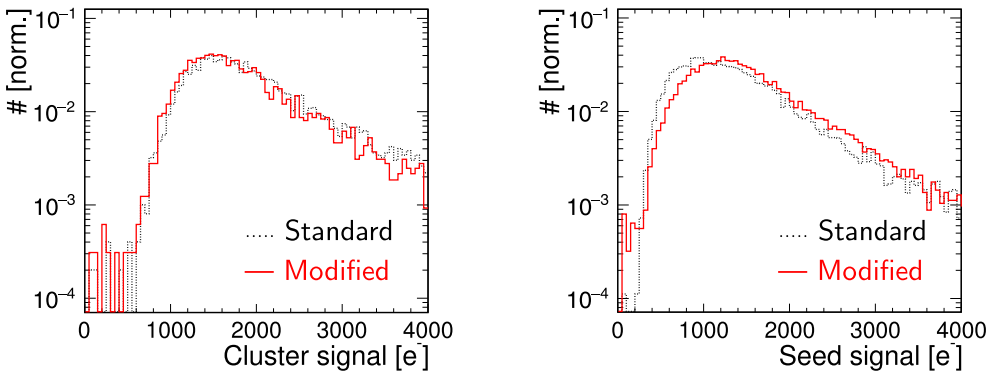

Fig. 9. *Cluster signal (left)* and *seed signal (right)* distribution for a bias voltage of −6 V.

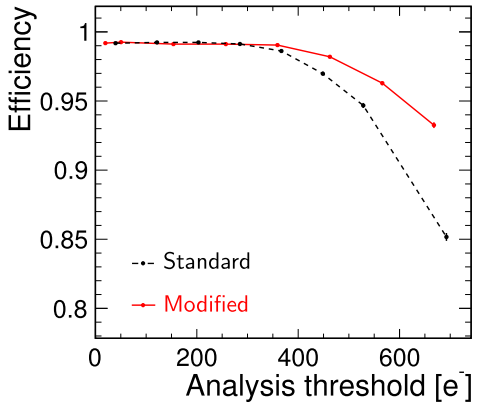

Fig. 10. Efficiency versus analysis threshold. The error bars correspond to the statistical uncertainties, as described in the text.

6.3. Signal and efficiency

The sum of the signal of all pixels in a cluster (*cluster signal*) is presented in the left plot of Fig. 9. The cluster signal distribution of the standard and modified process is very similar: this shows that there is no lack of charge collection in the non-depleted regions of the standard process.

The highest single pixel signal (*seed signal*, see right plot in Fig. 9) is however slightly lower for the standard process since more charge is shared with the neighbouring pixels. Consequently, the efficiency of the standard process starts to drop at lower threshold values, as visible in Fig. 10, resulting in a larger efficient operation window for the modified process.

At threshold values below $\lesssim 350\,e^-$, an efficiency of 99.2% ± 0.1(stat.) % has been measured for both processes.

A statistically significant lack of efficiency, at 99.2 %, is observed at low threshold values. The seed signal is reduced by charge sharing such that the lowest seed signal is expected for tracks that pass through the pixel corners. The uniform distribution of the efficiency within the pixel cell presented in Fig. 11 shows that the reduced efficiency for low threshold values cannot be attributed to a cut of the applied thresholds into the low energy tail of the seed signal distributions. Moreover, the homogeneous measurement of the efficiency across the pixel matrix (Fig. 12) shows, that the efficiency loss cannot be attributed to performance variations across the pixel matrix.

Possible explanations for this slight loss of efficiency could be fluctuations of the pedestal values that are used to calculate the signal height or issues of the data acquisition, such as random losses of generated trigger signals.

6.4. Timing

The timing residual is defined as the separation in time between the reconstructed Investigator hit and the associated track and is presented in Fig. 13 for both process variants. To obtain the timing resolution, a Gaussian function is fitted to the timing residual on a range that contains 99.7 % of all statistics. The timing resolution σ_{time} is extracted from the width σ_{Gauss} of this fit

$$\sigma_{\text{time}} = \sqrt{\sigma^2_{Gauss} - \sigma^2_{time,tele}} \tag{3}$$

unfolding the timing resolution of the telescope $\sigma_{time,tele} = 1.1$ ns [10]. A better timing resolution is expected for the modified process compared to the standard process due to the higher electric field in the sensor of the modified process [11]. This has been observed with a timing resolution of 5 ± 0.3 ns for the modified and 6 ± 0.5 ns for the standard process, but the measurement precision is limited by the 65 MHz of the ADCs.

The time taken by the signal of the seed pixel to rise from 10 % up to 90 % of its total amplitude (T_{10-90}) is presented in Fig. 14, showing

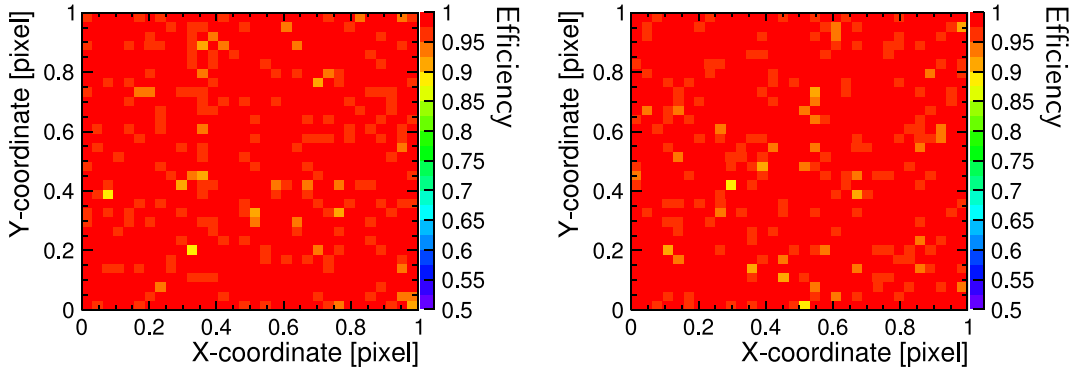

Fig. 11. In-pixel representation of the efficiency (colour online) for the *standard process (left)* and the *modified process (right)*.

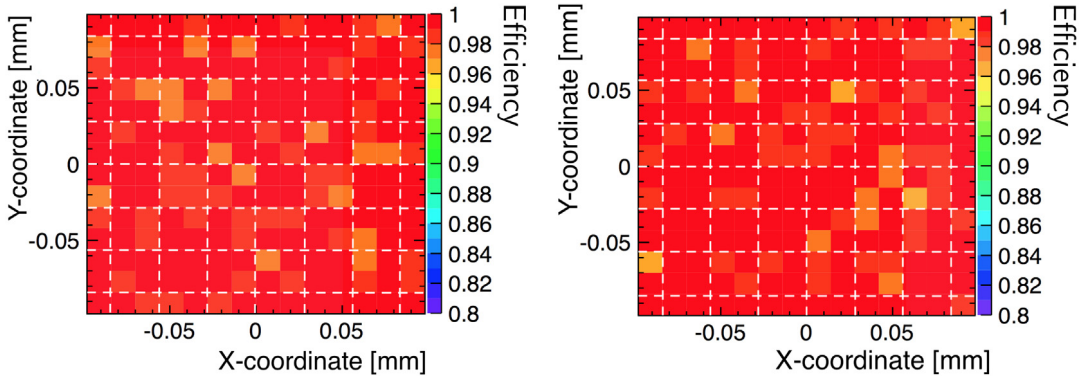

Fig. 12. Efficiency over the pixel matrix (colour online) for the *standard process (left)* and the *modified process (right)*. The white dashed lines mark the borders of a pixel cell.

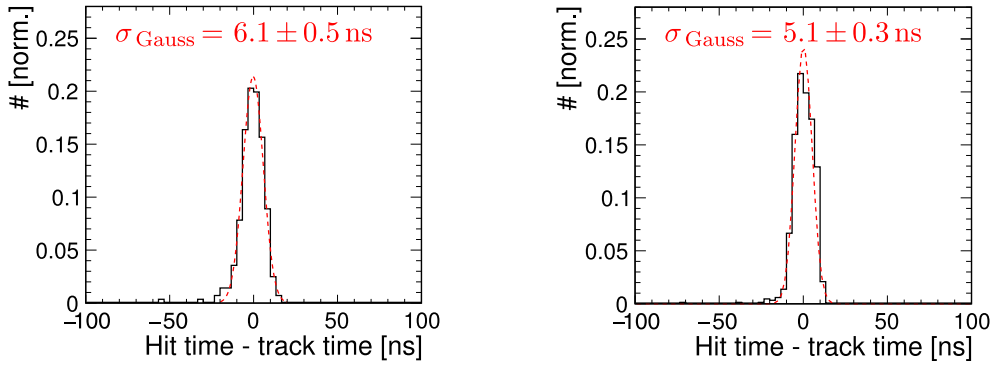

Fig. 13. Timing residual distribution for the *standard process (left)* and the *modified process (right)*. The red dashed lines mark the Gaussian fits.

a significantly delayed peak at $\sim$ 30 ns for the standard process, consistent with the slower charge collection in the non-depleted regions. This, as well as the observed width and tails of the time the signal takes to rise from 10 % up to 90 % of its total amplitude, might affect the timing resolution for technologies with an on-chip threshold and needs to be studied in more detail for a fully integrated chip in this technology.

7. Conclusions and outlook

A comparative study of two different CMOS process variants with a small collection electrode has been presented. The analogue performance of the laterally non-fully depleted standard process has been compared to the fully laterally depleted modified process for a pixel size of 28 µm and an epitaxial layer thickness of 25 µm. Significantly more charge sharing has been measured for the standard process than for the modified process, as expected from the non-depleted regions in the pixel edges and corners present in the standard process. The enhanced charge sharing for the standard process has several implications for the performance. The spatial resolution of down to ~3 µm for the standard process is significantly smaller than for the modified process, where a spatial resolution down to ~4 µm has been achieved. A smaller efficient operation window has been measured for different threshold values for the standard process, since the charge sharing reduces the seed signal, such that the efficiency of the standard process drops at lower threshold values.

The measured timing resolution of $\lesssim$ 6 ns for both processes is limited by the sampling frequency of the readout system used. A significantly slower rise time of ~30 ns has been measured for the standard process compared with the modified process (~18 ns). The slower rise time can affect the accuracy of the arrival time measurement in future fully integrated chips built in this technology, where the analogue waveform is digitised on-chip. Moreover, more refined measurements

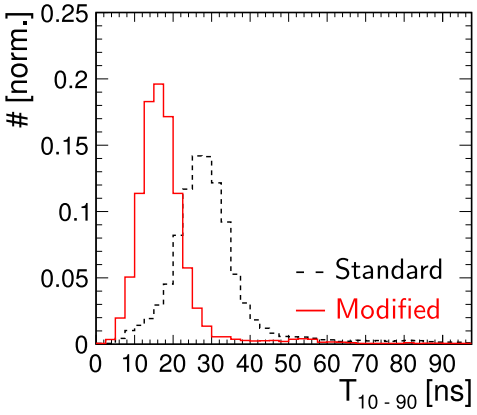

Fig. 14. T_{10-90} time distribution for the *standard process (black)* and the *modified process (red)*.

are needed, where the sampling frequency is not limiting the measured timing resolution.

Overall, the standard process is favourable in view of spatial resolution, while the modified process is favourable for faster charge collection and a larger window for efficient operation at higher threshold values.

Acknowledgements

This work has been sponsored by the Wolfgang Gentner Programme of the German Federal Ministry of Education and Research (grant no. 05E15CHA). It benefited from services provided by the ILC Virtual Organisation, supported by the national resource providers of the EGI

Federation and the research was done using resources provided by the Open Science Grid, which is supported by the National Science Foundation and the U.S. Department of Energy's Office of Science. The authors thank Fernando Duarte Ramos (CERN) for his support with the mechanical integration of the tested devices in the telescope system. The help from the staff operating the CERN SPS and the North Area test facilities is gratefully acknowledged.

References

[1] M. Aicheler, et al., A multi-TeV linear collider based on CLIC technology: CLIC conceptual design report, in: Tech. Rep. CERN-2012-007, Geneva, 2012 URL: https://cds.cern.ch/record/1500095.

[2] L. Linssen, et al., Physics and detectors at CLIC: CLIC conceptual design report, in: Tech. Rep. CERN-2012-003, Geneva, 2012 URL: http://cds.cern.ch/record/1425915.

[3] P. Lebrun, et al., The CLIC programme: Towards a staged e+e- linear collider exploring the terascale: CLIC conceptual design report, in: Tech. Rep. CERN-2012-005, Geneva, 2012 URL: http://cds.cern.ch/record/1475225.

[4] M. Boland, et al., Updated baseline for a staged compact linear collider, in: Tech. Rep. CERN-2016-004, Geneva, 2016 URL: http://cds.cern.ch/record/2210892.

[5] N.A. Tehrani, et al., CLICdet: The post-CDR CLIC detector model (CLICdp-Note-2017-001), URL: http://cds.cern.ch/record/2254048.

[6] A.M. Nurnberg, D. Dannheim, Requirements for the CLIC tracker readout (CLICdp-Note-2017-002), URL: https://cds.cern.ch/record/2261066.

[7] B. Abelev, et al., Technical design report for the upgrade of the ALICE inner tracking system, in: Tech. Rep. CERN-LHCC-2013-024, 2013, ALICE-TDR-017 URL: https://cds.cern.ch/record/1625842.

[8] J.W. van Hoorne, Study and Development of a novel silicon pixel detector for the upgrade of the ALICE inner tracking system, Ph.D. Thesis, 2015, presented URL: https://cds.cern.ch/record/2119197.

[9] W. Snoeys, et al., A process modification for CMOS monolithic active pixel sensors for enhanced depletion, timing performance and radiation tolerance, Nucl. Instrum. Methods Phys. Res. A 871 (Supplement C) (2017) 90–96, URL: http://www.sciencedirect.com/science/article/pii/S016890021730791X.

[10] N.A. Tehrani, Test-beam measurements and simulation studies of thin pixel sensors for the CLIC vertex detector, Ph.D. Thesis, 2017, URL: https://cds.cern.ch/record/2270788.

[11] M. Munker, Test beam and simulation studies on high resistivity cmos pixel sensors, Ph.D. Thesis, 2018, URL: https://cds.cern.ch/record/2644054.

[12] K.M. Sielewicz, Mitigation methods increasing radiation hardness of the FPGA-based readout of the ALICE inner tracking system, Ph.D. Thesis, 2018, URL: https://cds.cern.ch/record/2643800.

[13] ANALOG DEVICES, AD9249: 16 Channel 14-Bit, 65 MSPS, Serial LVDS, 18 V A/D Converter, 2013, URL: http://www.analog.com/media/en/technical-documentation/data-sheets/AD9249pdf.

[14] E. Belau, et al., Charge collection in silicon strip detectors, Nucl. Instrum. Methods Phys. Res. 214 (2) (1983) 253–260, URL: http://www.sciencedirect.com/science/article/pii/0167508783905914.